Original Article | Gastrointestinal Imaging

http://dx.doi.org/10.3348/kjr.2015.16.6.1216
pISSN 1229-6929 · eISSN 2005-8330
Korean J Radiol 2015;16(6):1216-1225

Korean Journal of Radiology
KJR

Reduced Field-of-View Diffusion-Weighted Magnetic Resonance Imaging of the Pancreas: Comparison with Conventional Single-Shot Echo-Planar Imaging

Hyungjin Kim, MD[1, 2], Jeong Min Lee, MD[1, 3], Jeong Hee Yoon, MD[1], Jin-Young Jang, MD[4], Sun-Whe Kim, MD[4], Ji Kon Ryu, MD[5], Stephan Kannengiesser, PhD[6], Joon Koo Han, MD[1, 3], Byung Ihn Choi, MD[1, 3]

Departments of [1]Radiology and [4]Surgery, Seoul National University Hospital, Seoul 03080, Korea; [2]Aerospace Medical Group, Air Force Education and Training Command, Jinju 52634, Korea; [3]Institute of Radiation Medicine, Seoul National University College of Medicine, Seoul 03080, Korea; [5]Division of Gastroenterology, Department of Internal Medicine, Seoul National University College of Medicine, Seoul 03080, Korea; [6]Siemens Healthcare, Erlangen, Germany

Objective: To investigate the image quality (IQ) and apparent diffusion coefficient (ADC) of reduced field-of-view (FOV) diffusion-weighted imaging (DWI) of pancreas in comparison with full FOV DWI.

Materials and Methods: In this retrospective study, 2 readers independently performed qualitative analysis of full FOV DWI (FOV, 38 x 38 cm; b-value, 0 and 500 s/mm^2) and reduced FOV DWI (FOV, 28 x 8.5 cm; b-value, 0 and 400 s/mm^2). Both procedures were conducted with a two-dimensional spatially selective radiofrequency excitation pulse, in 102 patients with benign or malignant pancreatic diseases (mean size, 27.5 ± 14.4 mm). The study parameters included 1) anatomic structure visualization, 2) lesion conspicuity, 3) artifacts, 4) IQ score, and 5) subjective clinical utility for confirming or excluding initially considered differential diagnosis on conventional imaging. Another reader performed quantitative ADC measurements of focal pancreatic lesions and parenchyma. Wilcoxon signed-rank test was used to compare qualitative scores and ADCs between DWI sequences. Mann Whitney U-test was used to compare ADCs between the lesions and parenchyma.

Results: On qualitative analysis, reduced FOV DWI showed better anatomic structure visualization (2.76 ± 0.79 at b = 0 s/mm^2 and 2.81 ± 0.64 at b = 400 s/mm^2), lesion conspicuity (3.11 ± 0.99 at b = 0 s/mm^2 and 3.15 ± 0.79 at b = 400 s/mm^2), IQ score (8.51 ± 2.05 at b = 0 s/mm^2 and 8.79 ± 1.60 at b = 400 s/mm^2), and higher clinical utility (3.41 ± 0.64), as compared to full FOV DWI (anatomic structure, 2.18 ± 0.59 at b = 0 s/mm^2 and 2.56 ± 0.47 at b = 500 s/mm^2; lesion conspicuity, 2.55 ± 1.07 at b = 0 s/mm^2 and 2.89 ± 0.86 at b = 500 s/mm^2; IQ score, 7.13 ± 1.83 at b = 0 s/mm^2 and 8.17 ± 1.31 at b = 500 s/mm^2; clinical utility, 3.14 ± 0.70) ($p < 0.05$). Artifacts were significantly improved on reduced FOV DWI (2.65 ± 0.68) at b = 0 s/mm^2 (full FOV DWI, 2.41 ± 0.63) ($p < 0.001$). On quantitative analysis, there were no significant differences between the 2 DWI sequences in ADCs of various pancreatic lesions and parenchyma ($p > 0.05$). ADCs of adenocarcinomas (1.061 x 10^{-3} mm^2/s ± 0.133 at reduced FOV and 1.079 x 10^{-3} mm^2/s ± 0.135 at full FOV) and neuroendocrine tumors (0.983 x 10^{-3} mm^2/s ± 0.152 at reduced FOV and 1.004 x 10^{-3} mm^2/s ± 0.153 at full FOV) were significantly lower than those of parenchyma (1.191 x 10^{-3} mm^2/s ± 0.125 at reduced FOV and 1.218 x 10^{-3} mm^2/s ± 0.103 at full FOV) ($p < 0.05$).

Conclusion: Reduced FOV DWI of the pancreas provides better overall IQ including better anatomic detail, lesion conspicuity and subjective clinical utility.

Index terms: *Reduced field-of-view; Image quality; Apparent diffusion coefficient; Diffusion-weighted imaging; Magnetic resonance imaging; Pancreas*

Received November 8, 2014; accepted after revision July 21, 2015.
This work was partly supported by a grant (No. 04-2011-0310) from the SNUH Research Fund, and by a grant from the National R&D Program for Cancer Control, Ministry for Health and Welfare, Republic of Korea (Contract grant number: 1120310).
Corresponding author: Jeong Min Lee, MD, Department of Radiology and Institute of Radiation Medicine, Seoul National University College of Medicine, 101 Daehak-ro, Jongno-gu, Seoul 03080, Korea.
• Tel: (822) 2072-3154 • Fax: (822) 743-6385 • E-mail: jmsh@snu.ac.kr

Korean Journal of Radiology
KJR

INTRODUCTION

Diffusion-weighted imaging (DWI) is based on the principles of the Brownian motion of water molecules, i.e., random microscopic motion. This random motion, which results in the diffusion of water molecules, decreases the magnetic resonance (MR) signal when diffusion-sensitizing gradients are applied, and is the basis of the image contrast observed on DWI (1). DWI is successfully applied to many organs; and recently, the application of DWI to the pancreas has been investigated in several studies on pancreatic neoplasms and inflammatory diseases (2-6). In addition, the apparent diffusion coefficient (ADC) from DWI, reflects the diffusivity of lesions. Previous studies indicated that the ADC values of pancreatic adenocarcinoma tend to be lower than those of normal pancreas (2-6), and, therefore, ADC could be useful for differentiating pancreatic malignancies from normal pancreatic tissue, although not for differentiating malignancies from other benign or inflammatory lesions (7, 8). In addition, DWI could provide comparable performance to conventional MRI for the detection of neuroendocrine tumors and is particularly superior in detecting small (0.5–1 cm) and non-hypervascular lesions (9). Inflammatory diseases such as acute pancreatitis are also assessed with DWI. Shinya et al. (10) reported that DWI could detect acute pancreatitis more clearly than CT without contrast enhancement. However, despite these various applications, the clear shortcomings of pancreas DWI include poor spatial resolution, ghosting, and susceptibility artifacts due to adjacent organs (11, 12).

Recently, DWI with reduced field-of-view (FOV) in the phase-encoding direction has been developed (13, 14). This new DWI sequence was initially applied to spinal cord imaging (13, 14), as this organ is relatively small and prone to distortions. However, this novel sequence allows focus on a single organ of interest instead of unnecessary imaging of whole upper abdominal spaces. Thus, the pancreas is also an attractive organ for this method. A few previous studies of reduced FOV DWI on pancreas showed that this new sequence leads to substantial improvement in image quality (IQ) with reduction of artifacts (15, 16). However, these studies included a small subset of patients and pancreatic pathologies were not specifically assessed (15, 16).

Thus, the purpose of our study was to perform qualitative comparisons of IQ and quantitative comparisons of ADC between reduced FOV and full FOV pancreas DWI sequences to evaluate the performance of reduced FOV DWI in patients with various pancreatic diseases. We also assessed whether reduced FOV DWI had clinical utility for differential diagnosis.

MATERIALS AND METHODS

This retrospective study was approved by the Institutional Review Board of Seoul National University Hospital with waiver of patients' informed consent.

Patients

Our radiology database was retrospectively searched between October 2011 and December 2012 to identify patients who were referred to our department for MRI examinations of the upper abdomen for biliary-pancreas evaluation. Patients were examined with the use of our biliary-pancreas MRI protocol including conventional full FOV DWI and reduced FOV DWI at 3T (Magnetom Verio, Siemens Medical Solutions, Erlangen, Germany) using a 32-channel phased-array coil. The study population was determined based on the following criteria: 1) patients with pancreatic diseases that were histopathologically confirmed after MRI; 2) pancreatic lesions larger than 1 cm;

Table 1. Final Diagnoses of 102 Pancreatic Lesions

Diagnosis	No. of Patients	Lesion Location				Size (mm)*
		Uncinate Process	Head	Body	Tail	
Adenocarcinoma	44 (43.1)	5 (11.4)	19 (43.2)	10 (22.7)	10 (22.7)	27.6 ± 11.5
Noninvasive IPMN	16 (15.7)	2 (12.5)	6 (37.5)	5 (31.3)	3 (18.8)	25.1 ± 7.3
IPMC	5 (4.9)	2 (40)	1 (20)	1 (20)	1 (20)	31.2 ± 22.2
Neuroendocrine tumor	18 (17.6)	1 (5.6)	7 (38.9)	2 (11.1)	8 (44.4)	21.7 ± 13.7
Serous cystic tumor	8 (7.8)	0 (0)	2 (25)	3 (37.5)	3 (37.5)	39.4 ± 26.6
Mucinous cystic tumor	3 (2.9)	0 (0)	0 (0)	0 (0)	3 (100)	42.2 ± 21.4
Others†	8 (7.8)	0 (0)	3 (37.5)	1 (12.5)	4 (50)	24.7 ± 10.5

Data are number of patients unless otherwise specified. Data in parentheses are percentages. *Data are mean ± standard deviation, †Benign epithelial cysts (n = 3), metastases (n = 2), schwannoma (n = 1), solid pseudopapillary tumor (n = 1), and desmoid tumor (n = 1) were included. IPMC = intraductal papillary mucinous carcinoma, IPMN = intraductal papillary mucinous neoplasm

3) no prior oncologic treatment such as chemotherapy or radiotherapy.

On the basis of the selection criteria, 102 patients (55 men and 47 women; mean age, 60.34 ± 11.73 years) were enrolled. Of these, 74 patients underwent surgery with the Whipple procedure or distal pancreatectomy, and 28 patients underwent only diagnostic biopsy. Detailed final diagnoses were presented in Table 1. The mean size of the enrolled pancreatic lesions was 27.5 ± 14.4 mm.

MR Examinations

Unenhanced T2- and T1-weighted images were obtained with the Half Fourier Single-shot Turbo Spin Echo sequence (HASTE) and the dual echo in- and opposed-phase Fast Low Angle Shot (FLASH) sequence techniques, respectively. MR cholangiography using 3 MR methods followed: 1) breath-hold single-section rapid acquisition with Turbo Spin Echo (TSE), 2) breath hold multi-section HASTE, and 3) respiratory-triggered multisection three-dimensional (3D) TSE (17).

Dynamic images were obtained with a fat-suppressed 3D FLASH sequence; volume interpolation with breath-hold examinations (VIBE, Siemens Medical Solutions, Erlangen, Germany) before and after administration of gadobutrol (Gadovist; Bayer Schering Pharma AG, Berlin, Germany 0.1 mmol/kg of body weight at an injection rate of 1 mL/sec and injection duration of approximately 5 seconds). Acquisition of 3D VIBE for each phase was completed during a single breath-hold at the end of expiration (18–20 seconds). Precontrast images were obtained first, and arterial, portal venous, and equilibrium phase images were obtained at approximately 20–40 seconds, 45–65 seconds, and 3–5 minutes, respectively, after injection of the contrast agent.

DWI Acquisition

Two-dimensional (2D), fat-suppressed, respiratory-triggered, echo-planar DWI sequences were acquired in the axial plane before contrast injection. For full FOV DWI, generalized autocalibrating partially parallel acquisitions (Siemens Medical Solutions, Erlangen, Germany) with an acceleration factor of 3 was used. Three perpendicular

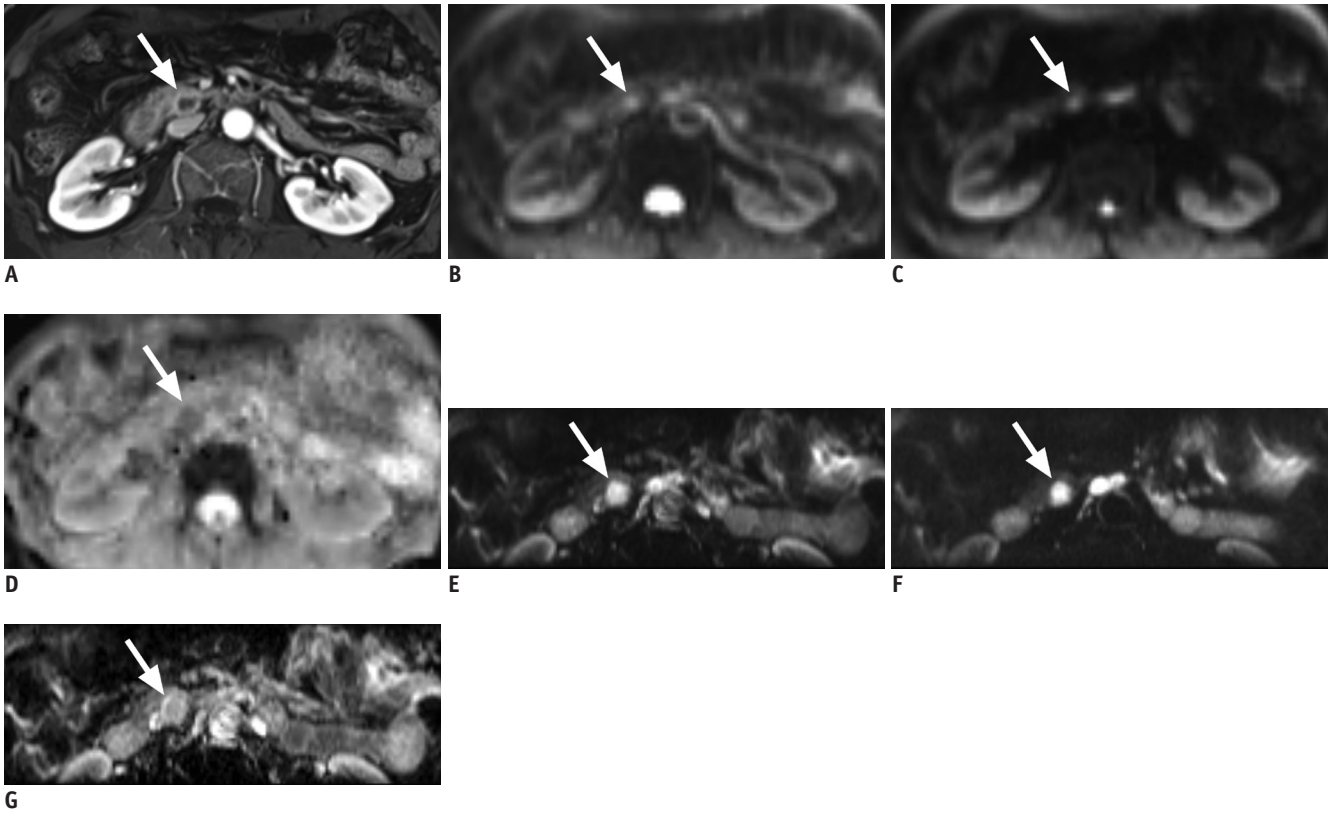

Fig. 1. 58-year-old woman with 1.5 cm sized neuroendocrine tumor (arrow) in pancreas uncinate process.
A. Mass shows rim enhancement on enhanced T1-weighted image. **B.** Full field-of-view (FOV) diffusion-weighted imaging (DWI) sequence at b = 0 s/mm^2. Lesion shows ill-defined hyperintensity. **C.** Full FOV DWI at b = 500 s/mm^2. Note that margin of lesion is severely blurred and barely delineable from background. **D.** Corresponding apparent diffusion coefficient (ADC) map of full FOV DWI. **E.** Reduced FOV DWI at b = 0 s/mm^2. **F.** Reduced FOV DWI at b = 400 s/mm^2. Lesion is more clearly visualized on reduced FOV image. **G.** Corresponding ADC map of reduced FOV DWI.

Korean Journal of Radiology
KJR

spatial directions were encoded with multiple b-values (0, 25, 50, 75, 100, 150, 200, 500, 800, 1000 s/mm^2 or 0, 25, 50, 75, 100, 150, 200, 500, 1500 s/mm^2). The selection of the number of b-values in our hospital was based on the previous studies (18, 19). A prototype sequence delivered by the manufacturer (Siemens Medical Solutions, Erlangen, Germany) was used for reduced FOV DWI that was performed with a 2D spatially selective radiofrequency (RF) excitation pulse to reduce the FOV in the phase-encoding direction (Fig. 1). The 2D RF pulse is based on a bipolar planar k-space trajectory, with an analytical pulse shape design approach similar that reported by Alley et al. (20). This pulse provides independent control of slice thickness and field of excitation in the phase-encoding direction and the prototype sequence allows FOV in phase-encoding direction down to 12.5%. The duration of the 2D RF excitation pulse for the reduced FOV protocol was 13.2 ms, while the corresponding one-dimensional RF excitation pulse of the full FOV protocol had a duration of 4.6 ms. Images of reduced FOV DWI were acquired with b-values of 0, 400, and 800 s/mm^2. Post-processing software automatically produced ADC maps. In addition, the reduced FOV protocol had a slightly higher specific absorption rate of 0.64 W/kg than full FOV DWI (0.56 W/kg). Detailed imaging parameters were listed in Table 2.

Image Analysis

Qualitative Analysis

Independent, qualitative image analysis was performed by 2 board-certified abdominal radiologists (with 22 and 7 years of experience in interpreting MR images, respectively). The reviewers were blinded to the patients' information including the pathology and lesion location. All image analyses were performed using picture archiving and communication system software (Maroview 5.4; Infinitt, Seoul, Korea) on a commercial workstation (xw6200; Hewlett-Packard, Palo Alto, CA, USA), with 2, 2048 x 1536-pixel, 20.8-inch monochrome liquid crystal display monitors (ME315L; Totoku Electric, Tokyo, Japan). Both DWI sequences were analyzed using a 4-point scale (1-4) for 1) anatomic structure visualization (1, poorly visualized anatomy and non-diagnostic; 2, fairly delineated pancreas with margin blurring; 3, good delineation of pancreas with a sharp margin; 4, excellent sharpness of the pancreas or clear visualization of the pancreatic duct), 2) pancreatic lesion conspicuity (1, lesion not detectable; 2, merely recognizable lesion-to-background contrast; 3, intermediate lesion-to-background contrast or high contrast with indistinct lesion margin; 4, excellent lesion-to-background contrast and a clear lesion margin), 3) presence of ghosting, motion or susceptibility artifacts (1, severe and non-diagnostic; 2, moderate; 3, mild; 4, absent), and 4) total IQ score as a sum of the aforementioned 3 parameters (21). Readers first evaluated only the full FOV DWI images and subsequently, the reduced FOV DWI using the same criteria. For each DWI, b = 0 s/mm^2 images were analyzed first, followed by high b-value images (b = 400 s/mm^2 for reduced FOV and b = 500 s/mm^2 for full FOV DWI). Thus, reviewers subjectively assigned a qualitative image analysis score for each DWI for each b-value (b = 0 s/mm^2 or b = 400 s/mm^2 for reduced FOV and b = 500 s/mm^2 for full FOV DWI).

After assessing the IQ, readers reviewed anatomic imaging including unenhanced T1-, T2-weighted images, as well as dynamic imaging. The readers were then asked to evaluate the subjective clinical utility of DWI for characterizing

Table 2. MR Imaging Parameters

	Reduced FOV	Full FOV
TR/TE (ms)	3200/70	5000/70
FOV (cm)	28 x 8.5	38 x 38
Matrix size	192 x 35	136 x 136
In-plane resolution (mm)	1.5 x 2.4	2.8 x 2.8
Section thickness (mm)	5	8
Slice number	15	22
Intersection gap (%)	10	0
Flip angle (degree)	90	90
NEX	6	3
B-value (s/mm^2)	0, 400, 800	0, 25, 50, 75, 100, 150, 200, 500, 800, 1000 or 0, 25, 50, 75, 100, 150, 200, 500, 1500
Acquisition time	2 min 18 sec	6 min 30 sec or 7 min 15 sec

FOV = field-of-view, NEX = number of excitations, TE = echo time, TR = repetition time

detected lesions as benign or malignant (they were not asked to specifically diagnose each focal pancreatic lesion). For lesion characterization, images with b-values of 0, 400, or 500 and other high-b-values (b = 800 s/mm^2 for reduced FOV and b = 800–1500 s/mm^2 for full FOV DWI) were analyzed for lesion morphology, signal intensity, degree of signal intensity decrease with increasing b-values, and qualitative assessment of ADC maps. Furthermore, a lesion was considered benign (mostly cystic lesions) if it was hyperintense on DWI at b = 0 sec/mm^2, with a strong signal intensity decrease at high b-value and an ADC that was subjectively higher than that of the surrounding pancreas parenchyma (2, 22). A lesion was considered malignant (mostly adenocarcinoma and neuroendocrine tumor) if it was mildly to moderately hyperintense on DWI at b = 0 sec/mm^2 and remained hyperintense, as compared with pancreas parenchyma at high b-value, with an ADC qualitatively lower than that of the surrounding parenchyma (3-6, 9). A lesion was considered indeterminate if the above criteria were not met (e.g., if there was a partial signal intensity decrease or isointense ADC). Thereafter, subjective clinical utility of DWI for confirmation or exclusion of initially considered differential diagnosis on conventional imaging was scored with a 4 point scale (23): 1, DWI was not useful for the differential diagnosis of pancreatic lesions as the lesion characterization on DWI was indeterminate or the lesion was invisible; 2, lesion characterization on DWI was consistent with the confirmed diagnostic impression on conventional imaging; 3, DWI helped to confirm the suspected diagnosis on conventional imaging; 4, DWI helped to characterize the lesion as benign or malignant when the conventional imaging findings were indeterminate for characterization (23).

Quantitative Analysis

Quantitative measurements of the ADC values of pancreas lesions and pancreatic parenchyma were independently performed by a single different radiologist with 4 years of experience in radiology under supervision of the corresponding author. Enhanced T1-weighted images were available for better detection of lesions, if required. The ADC values of the pancreas lesion and pancreas parenchyma were obtained by manually placing a circular region of interest (ROI) on the ADC maps acquired from both the reduced and full FOV DWI sequences. ROIs were placed at near-identical locations on both sequences with care to avoid vessels, cysts, bile ducts, and pancreatic ducts. Effort was made to have 3 ROIs in the lesions, as well as in the pancreas parenchyma. The mean size of the ROIs was 61.5 ± 30.6 mm^2 (range, 23.0–168.0 mm^2) for reduced

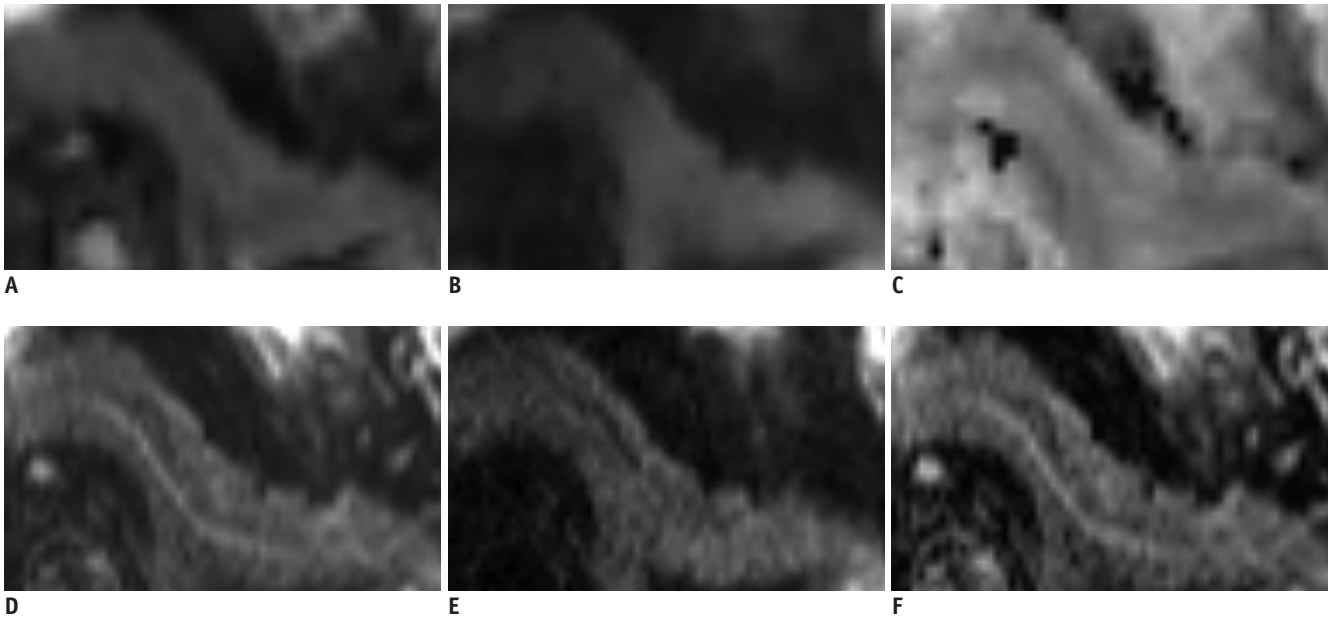

Fig. 2. 38-year-old man with neuroendocrine tumor (not shown) in pancreas tail.
Images are cropped to focus on pancreas. **A.** Full field-of-view (FOV) diffusion-weighted imaging (DWI) sequence at b = 0 s/mm^2. Margin of pancreas is blurred and duct is not visible. Normal lobulated appearance of pancreas is hardly recognizable. **B.** Full FOV DWI at b = 500 s/mm^2. **C.** Corresponding apparent diffusion coefficient (ADC) map of full FOV DWI. **D.** Reduced FOV DWI at b = 0 s/mm^2. Note that lobulated appearance of pancreas border and pancreatic duct are more clearly visualized on reduced FOV image. **E.** Reduced FOV DWI at b = 400 s/mm^2. **F.** Corresponding ADC map of reduced FOV DWI.

Korean Journal of Radiology
KJR

FOV and 69.5 ± 28.9 mm^2 (range, 23.0–101.5 mm^2) for full FOV images. For ADC measurement of pancreatic lesions, only lesions > 2 cm were measured in order to avoid sampling error. Images with low signal-to-noise ratio (SNR) and/or artifacts were excluded from measurement and patients with several miscellaneous diseases such as benign epithelial cysts, metastases, schwannomas, solid pseudopapillary tumors, and desmoid tumors were also excluded. Therefore, quantitative analysis of pancreatic lesions was performed in 26 patients with adenocarcinoma, 7 patients with noninvasive intraductal papillary mucinous neoplasm (IPMN), 3 patients with intraductal papillary mucinous carcinoma (IPMC), 7 patients with neuroendocrine tumor, 6 patients with serous cystic tumor, and 3 patients with mucinous cystic tumor. In terms of the analysis of pancreatic parenchyma, we strictly confined measurement to the normal parenchyma based on the following criteria: 1) no evidence of ductal obstruction in the head or body; 2) no parenchymal atrophy disrupting ROI placement; 3) no significant imaging artifacts and/or abnormally low SNR. Consequently, quantitative analysis of pancreatic parenchyma was performed in 27 patients.

Statistical Analysis

The Wilcoxon signed-rank test was used to compare the qualitative image analysis scores between reduced FOV and full FOV DWI sequences. Comparisons were made using the average scores between the 2 readers. Inter-reader agreement for qualitative evaluation was assessed using weighted κ statistics. Inter-reader agreement was considered as slight for κ = 0.00–0.20, fair for κ = 0.21–0.40, moderate for κ = 0.41–0.60, substantial for κ = 0.61–0.80, and almost perfect for κ = 0.81–1.00 (24). ADC values of various diseases and pancreas parenchyma were also compared between the 2 DWI sequences using the Wilcoxon signed-rank test. The Mann Whitney U-test was performed for comparisons of the ADCs between lesions and parenchyma, and the Kruskal-Wallis test was used for comparisons of ADCs among solid tumors and cystic lesions.

All statistical analyses were performed using 2 commercial software programs (MedCalc version 12.3.0, MedCalc Software, Mariakerke, Belgium; and SPSS 19.0, IBM SPSS Statistics, Armonk, NY, USA). A p value < 0.05 was considered as statistical significance.

RESULTS

Qualitative Image Quality Analysis

Reduced FOV DWI showed significantly better scores in anatomic structural visualization (2.76 ± 0.79 at b = 0 s/

Table 3. Qualitative Image Analysis Scores Compared between Reduced FOV and Full FOV Diffusion-Weighted Imaging Sequences

	Anatomic Structures	Lesion Conspicuity	Artifacts	Total Image Quality Score	Subjective Clinical Utility†
Reduced FOV (b = 0 s/mm^2)					
Reader 1	2.95 ± 0.83	3.19 ± 0.99	2.79 ± 0.78	8.93 ± 2.20	3.40 ± 0.68
Reader 2	2.57 ± 0.91	2.99 ± 1.14	2.50 ± 0.71	8.06 ± 2.16	3.44 ± 0.75
Average	2.76 ± 0.79	3.11 ± 0.99	2.65 ± 0.68	8.51 ± 2.05	3.41 ± 0.64
Full FOV (b = 0 s/mm^2)					
Reader 1	2.20 ± 0.63	2.55 ± 1.10	2.41 ± 0.74	7.16 ± 2.03	2.87 ± 0.86
Reader 2	2.16 ± 0.69	2.55 ± 1.21	2.40 ± 0.69	7.11 ± 1.87	3.40 ± 0.77
Average	2.18 ± 0.59	2.55 ± 1.07	2.41 ± 0.63	7.13 ± 1.83	3.14 ± 0.70
P value*	< 0.001	< 0.001	< 0.001	< 0.001	< 0.001
Reduced FOV (b = 400 s/mm^2)					
Reader 1	2.89 ± 0.69	3.09 ± 0.95	2.95 ± 0.65	8.93 ± 1.74	
Reader 2	2.74 ± 0.69	3.21 ± 0.89	2.71 ± 0.67	8.65 ± 1.78	
Average	2.81 ± 0.64	3.15 ± 0.79	2.83 ± 0.57	8.79 ± 1.60	
Full FOV (b = 500 s/mm^2)					N/A
Reader 1	2.47 ± 0.50	2.70 ± 0.90	2.62 ± 0.56	7.78 ± 1.45	
Reader 2	2.65 ± 0.62	3.09 ± 1.00	2.82 ± 0.53	8.56 ± 1.47	
Average	2.56 ± 0.47	2.89 ± 0.86	2.72 ± 0.45	8.17 ± 1.31	
P value*	< 0.001	0.002	0.061	< 0.001	

Data are mean ± standard deviation. *Wilcoxon signed-rank test was performed between reduced FOV and full FOV sequences using averaged image quality scores of two readers, †Scoring of subjective clinical utility was performed once for each DWI sequence. DWI = diffusion-weighted imaging, FOV = field-of-view, N/A = not available

mm^2 and 2.81 ± 0.64 at b = 400 s/mm^2) (Fig. 2), lesion conspicuity (3.11 ± 0.99 at b = 0 s/mm^2 and 3.15 ± 0.79 at b = 400 s/mm^2) and total IQ score (8.51 ± 2.05 at b = 0 s/mm^2 and 8.79 ± 1.60 at b = 400 s/mm^2), as compared to full FOV DWI (anatomic structure, 2.18 ± 0.59 at b = 0 s/mm^2 and 2.56 ± 0.47 at b = 500 s/mm^2; lesion conspicuity, 2.55 ± 1.07 at b = 0 s/mm^2 and 2.89 ± 0.86 at b = 500 s/mm^2; IQ score, 7.13 ± 1.83 at b = 0 s/mm^2 and 8.17 ± 1.31 at b = 500 s/mm^2) (all $p < 0.05$). In addition, the subjective clinical utility of reduced FOV DWI (3.41 ± 0.64) was also higher than that of full FOV DWI (3.14 ± 0.70) ($p < 0.001$). MR artifacts were significantly improved on reduced FOV DWI (2.65 ± 0.68) at b = 0 s/mm^2 (full FOV DWI, 2.41 ± 0.63) ($p < 0.001$), however, no significant difference was noted between reduced FOV (2.83 ± 0.57) and full FOV DWI (2.72 ± 0.45) at b = 400 or 500 s/mm^2 ($p = 0.061$). Detailed data were shown in Table 3.

Overall agreement between the 2 reviewers was fair to substantial (Table 4), and weighted κ between the reviewers ranged from 0.355 to 0.660 for reduced FOV DWI and from 0.251 to 0.618 for full FOV DWI, respectively.

Quantitative ADC Measurements of Pancreas Lesions and Parenchyma

There were no significant differences between reduced FOV and full FOV DWI in the ADC values of various pancreatic lesions and pancreatic parenchyma (all $p > 0.05$) (Table 5). ADC values of pancreatic adenocarcinomas (1.061 x 10^{-3} mm^2/s ± 0.133 at reduced FOV and 1.079 x 10^{-3} mm^2/s ± 0.135 at full FOV) and neuroendocrine tumors (0.983 x 10^{-3} mm^2/s ± 0.152 at reduced FOV and 1.004 x 10^{-3} mm^2/s ± 0.153 at full FOV) were significantly lower than those of pancreas parenchyma (1.191 x 10^{-3} mm^2/s ± 0.125 at reduced FOV and 1.218 x 10^{-3} mm^2/s ± 0.103 at full FOV) (reduced FOV, $p < 0.001$ and $p = 0.001$, respectively; full FOV, $p < 0.001$ and $p = 0.003$, respectively). However, ADC values measured at the solid portion of IPMCs (1.160 x 10^{-3} mm^2/s ± 0.046 at reduced FOV and 1.208 x 10^{-3} mm^2/s ± 0.088 at full FOV) were not significantly different from the parenchyma (reduced FOV, $p = 0.695$; full FOV, $p = 0.897$). In addition, ADC values of cystic lesions such as noninvasive IPMNs (2.620 x 10^{-3} mm^2/s ± 0.252 at reduced FOV and 2.679 x 10^{-3} mm^2/s ± 0.337 at full FOV), serous cystic tumors

Table 4. Weighted κ Statistics for Inter-Reader Agreement of Qualitative Image Quality Scores

	Reduced FOV		Full FOV	
	b = 0 s/mm^2	b = 400 s/mm^2	b = 0 s/mm^2	b = 500 s/mm^2
Anatomic structures	0.473 (0.352, 0.594)	0.613 (0.493, 0.732)	0.561 (0.418, 0.703)	0.365 (0.219, 0.512)
Lesion conspicuity	0.660 (0.554, 0.767)	0.355 (0.227, 0.483)	0.618 (0.511, 0.726)	0.461 (0.346, 0.576)
Artifacts	0.496 (0.376, 0.616)	0.388 (0.241, 0.534)	0.431 (0.284, 0.578)	0.251 (0.096, 0.405)
Total image quality score	0.543 (0.443, 0.644)	0.490 (0.386, 0.593)	0.564 (0.474, 0.654)	0.382 (0.278, 0.485)
Subjective clinical utility	0.470 (0.312, 0.627)		0.305 (0.165, 0.445)	

Data in parentheses are 95% confidence intervals. FOV = field-of-view

Table 5. Apparent Diffusion Coefficient Measurements and Comparisons between Reduced Field-of-View (FOV) and Full FOV Diffusion-Weighted Imaging Sequences

	Reduced FOV (x 10^{-3} mm^2/s)	Full FOV (x 10^{-3} mm^2/s)	*P**
Adenocarcinoma (n = 26)	1.061 ± 0.133	1.079 ± 0.135	0.438
Noninvasive IPMN (n = 7)	2.620 ± 0.252	2.679 ± 0.337	0.176
IPMC (n = 3)	1.160 ± 0.046	1.208 ± 0.088	0.285
Neuroendocrine tumor (n = 7)	0.983 ± 0.152	1.004 ± 0.153	0.499
Serous cystic tumor (n = 6)	2.607 ± 0.277	2.582 ± 0.289	0.463
Mucinous cystic tumor (n = 3)	2.709 ± 0.455	2.736 ± 0.346	0.593
Pancreas parenchyma (n = 27)	1.191 ± 0.125	1.218 ± 0.103	0.070

Data are mean ± standard deviation. *Wilcoxon signed-rank test was performed. IPMC = intraductal papillary mucinous carcinoma, IPMN = intraductal papillary mucinous neoplasm

Korean Journal of Radiology
KJR

(2.607×10^{-3} mm^2/s ± 0.277 at reduced FOV and 2.582×10^{-3} mm^2/s ± 0.289 at full FOV), and mucinous cystic tumors (2.709×10^{-3} mm^2/s ± 0.455 at reduced FOV and 2.736×10^{-3} mm^2/s ± 0.346 at full FOV) were significantly higher than those of parenchyma on both DWI sequences (all $p < 0.001$). When ADC values were compared among solid tumors of adenocarcinoma, IPMC and neuroendocrine tumor, there were no significant differences on both DWI sequences (reduced FOV, $p = 0.075$; full FOV, $p = 0.115$). Likewise, among cystic lesions of the pancreas, there were no significant differences on both DWI sequences (reduced FOV, $p = 0.664$; full FOV, $p = 0.734$). Detailed data regarding ADC values were provided in Table 5.

DISCUSSION

In this study, we comparatively analyzed the IQ of reduced FOV DWI vs. conventional full FOV DWI, in order to evaluate the focal pancreatic lesions and parenchyma. The results indicated that reduced FOV DWI shows better anatomic structural visualization, lesion conspicuity, total IQ as well as subjective clinical utility. In addition, image artifacts were decreased on reduced FOV at both b-values, although a statistical difference between the sequences was seen only at b = 0 s/mm^2. We also demonstrated that the ADC values of pancreatic lesions and parenchyma on reduced FOV DWI were generally equivalent to those on full FOV DWI. Our study results were in agreement with the previous studies (15, 16). Although previous studies demonstrated that reduced FOV DWI of the pancreas could produce superior subjective IQ, and generally similar ADC values (15, 16), as compared to full FOV DWI, they were limited by a small number of patients (n = 10) with focal pancreatic lesions (15) or absence of any focal pancreatic lesions. On the other hand, our study included a much larger study population (n = 102) involving various pancreatic diseases including both benign and malignant conditions. We also confirmed the usefulness of reduced FOV DWI as an added utility to conventional MR imaging for the differential diagnosis of pancreatic lesions. Reduced FOV DWI has previously been applied to other organs including the optic nerve, breast, spinal cord, and prostate gland (13, 14, 25-28); in addition, better IQ (14, 26), added clinical value (23) and more accurate detection of small focal lesions (25, 26) with reduced FOV DWI has been reported. Our study results were consistent with the previous research results; furthermore, we found that reduced FOV DWI would also be beneficial for the pancreas.

In the present study, qualitative analysis indicated that the visualization of anatomic detail is a notable strength of reduced FOV DWI. Both readers assigned scores of '4' (excellent sharpness of the pancreas or clear visualization of the pancreatic duct) to 13 cases on b = 0 s/mm^2 and to 7 cases on b = 400 s/mm^2. However, none of the cases received a score of '4' on full FOV DWI for anatomic structural visualization on both b-values. The in-plane resolution of reduced FOV image was approximately 2.2-fold higher than that of full FOV DWI, which probably contributed to the better visualization of anatomic structures. Reduced FOV DWI earned significantly higher scores for lesion conspicuity than full FOV DWI. Since DWI may work as an especially useful modality for detecting iso-intense or iso-attenuating pancreas adenocarcinomas (29, 30), a small but important subset, improved lesion conspicuity on reduced FOV DWI has clinical significance. In addition, the advantages of reduced FOV DWI for lesion detection would likely be more substantial for smaller lesions. Our study only included lesions > 1 cm, hence, further research with smaller lesions is required.

Reduced FOV DWI earned higher mean scores for imaging artifacts than full FOV DWI, although the difference between 2 sequences was not significant at the higher b-values (b = 400 or 500 s/mm^2). Reduced imaging distortions could be achieved by decreased number of acquisition steps and reduction in the echo-planar imaging (EPI) echo train without increase in scan time on reduced FOV DWI with spatially selective RF pulse (16, 31). In addition, with 2 independent transmit channels, the RF pulses could be optimized for a more homogeneous flip angle distribution through incorporation of B1 field information into the RF pulse calculation (16). Excluding air-tissue interfaces from the shim volume would also reduce susceptibility-induced artifacts (26). Furthermore, reduction of the required number of k-space lines in the phase-encoding direction would enable higher resolution imaging for a fixed scan time (13). As pancreas imaging is often disturbed by adjacent air in the stomach and the motion of abdominal organs and aorta during scanning, reduced FOV DWI potentially has strong advantages over conventional single shot EPI. Our study results suggested that the pancreas is a very suitable organ for the application of the reduced FOV DWI, since it lies horizontally to the x axis of the transverse body plane. Thus, a reduced FOV DWI could be included in the pancreas protocol MRI.

Quantitative analysis indicated no significant differences between the 2 DWI sequences in the ADC measurements of pancreatic lesions and parenchyma, as previously reported in the literature (14, 15, 26). ADC values of pancreatic adenocarcinomas and neuroendocrine tumors were significantly lower than those of pancreas parenchyma and mean ADC values of neuroendocrine tumors were lower than those of adenocarcinomas, although no significant differences were noted between the 2 diseases. The histologic grade was a possible reason for the low ADC values of neuroendocrine tumors in our study (32). Among 7 patients with neuroendocrine tumors, 5 patients had a grade 2 and 1 patient had a grade 3 tumor.

We used a 2D spatially selective RF excitation pulse for the acquisition of reduced FOV DWI in our study. There are several other approaches for reduced FOV DWI, which consist of mainly suppressing or dephasing the signal intensity outside of the desired FOV rather than exciting only the targeted ROI (27, 28, 33, 34). These methods were applied to the imaging of spinal cords and optic nerves (27, 28, 33, 34). However, Zaharchuk et al. (14), reported that these approaches may be suboptimal in the setting of motion or magnetic field inhomogeneities. Thus, it is not easy to exploit these techniques in evaluation of the pancreas.

Apart from the intrinsic limits of any retrospective study, our study had several other limitations. First, a limited spectrum of diseases was included in the study. Imaging of benign diseases such as focal pancreatitis other than malignant neoplasms may provide additional information including lesion detectability and artifacts in the setting of peri-pancreatic inflammation. Second, b-values used in the analysis of reduced FOV were b = 0 and 400 s/mm^2 and those used in full FOV DWI were b = 0 and 500 s/mm^2. Such a difference in b-value might have affected ADC value measurements, as well as the qualitative image analysis. Furthermore, the difference in the series of b-values (3 b-values for reduced FOV and 9–10 b-values for full FOV DWI) in image acquisition between the protocols and the subsequent disparity in the acquisition time might have affected the overall IQ. Such heterogeneity between the protocols occurred as full FOV DWI with multiple b-values was originally a routine sequence of the biliary-pancreas MRI in our hospital, while reduced FOV DWI was implemented more recently as a prototype sequence according to the manufacturer's recommendations. Further study with equal b-values and other imaging parameters is required. Third, the inter-reader agreement of qualitative analysis was only fair to substantial. As qualitative analysis was performed by the 2 readers independently and was not consensus-driven, discrepancy in a few cases was inevitable. Zaharchuk et al. (14), who dealt with the reduced FOV DWI of human spinal cord, also reported that the weighted κ between the 2 reviewers for the evaluation of susceptibility, resolution, SNR, anatomy, and clinical utility ranged from 0.45 to 0.59, which was comparable to that in our study. A substantial training session prior to the investigation would be required in future studies.

In conclusion, compared to full FOV DWI, reduced FOV DWI of the pancreas provides higher overall IQ as well as better anatomical structure delineation, lesion conspicuity and subjective clinical utility. The greater than 2-fold higher spatial resolution of reduced FOV DWI would help radiologists better evaluate pancreatic diseases in greater detail.

Acknowledgments

We thank Chris Woo for his editorial assistance.

REFERENCES

1. Koh DM, Collins DJ. Diffusion-weighted MRI in the body: applications and challenges in oncology. *AJR Am J Roentgenol* 2007;188:1622-1635
2. Balci NC, Perman WH, Saglam S, Akisik F, Fattahi R, Bilgin M. Diffusion-weighted magnetic resonance imaging of the pancreas. *Top Magn Reson Imaging* 2009;20:43-47
3. Fattahi R, Balci NC, Perman WH, Hsueh EC, Alkaade S, Havlioglu N, et al. Pancreatic diffusion-weighted imaging (DWI): comparison between mass-forming focal pancreatitis (FP), pancreatic cancer (PC), and normal pancreas. *J Magn Reson Imaging* 2009;29:350-356
4. Kartalis N, Lindholm TL, Aspelin P, Permert J, Albiin N. Diffusion-weighted magnetic resonance imaging of pancreas tumours. *Eur Radiol* 2009;19:1981-1990
5. Lee SS, Byun JH, Park BJ, Park SH, Kim N, Park B, et al. Quantitative analysis of diffusion-weighted magnetic resonance imaging of the pancreas: usefulness in characterizing solid pancreatic masses. *J Magn Reson Imaging* 2008;28:928-936
6. Matsuki M, Inada Y, Nakai G, Tatsugami F, Tanikake M, Narabayashi I, et al. Diffusion-weighed MR imaging of pancreatic carcinoma. *Abdom Imaging* 2007;32:481-483
7. Sandrasegaran K, Nutakki K, Tahir B, Dhanabal A, Tann M, Cote GA. Use of diffusion-weighted MRI to differentiate chronic pancreatitis from pancreatic cancer. *AJR Am J Roentgenol* 2013;201:1002-1008
8. Wiggermann P, Grützmann R, Weissenböck A, Kamusella P,

Dittert DD, Stroszczynski C. Apparent diffusion coefficient measurements of the pancreas, pancreas carcinoma, and mass-forming focal pancreatitis. *Acta Radiol* 2012;53:135-139
9. Anaye A, Mathieu A, Closset J, Bali MA, Metens T, Matos C. Successful preoperative localization of a small pancreatic insulinoma by diffusion-weighted MRI. *JOP* 2009;10:528-531
10. Shinya S, Sasaki T, Nakagawa Y, Guiquing Z, Yamamoto F, Yamashita Y. The efficacy of diffusion-weighted imaging for the detection and evaluation of acute pancreatitis. *Hepatogastroenterology* 2009;56:1407-1410
11. Bittencourt LK, Matos C, Coutinho AC Jr. Diffusion-weighted magnetic resonance imaging in the upper abdomen: technical issues and clinical applications. *Magn Reson Imaging Clin N Am* 2011;19:111-131
12. Dietrich O, Biffar A, Baur-Melnyk A, Reiser MF. Technical aspects of MR diffusion imaging of the body. *Eur J Radiol* 2010;76:314-322
13. Saritas EU, Cunningham CH, Lee JH, Han ET, Nishimura DG. DWI of the spinal cord with reduced FOV single-shot EPI. *Magn Reson Med* 2008;60:468-473
14. Zaharchuk G, Saritas EU, Andre JB, Chin CT, Rosenberg J, Brosnan TJ, et al. Reduced field-of-view diffusion imaging of the human spinal cord: comparison with conventional single-shot echo-planar imaging. *AJNR Am J Neuroradiol* 2011;32:813-820
15. Ma C, Li YJ, Pan CS, Wang H, Wang J, Chen SY, et al. High resolution diffusion weighted magnetic resonance imaging of the pancreas using reduced field of view single-shot echo-planar imaging at 3 T. *Magn Reson Imaging* 2014;32:125-131
16. Riffel P, Michaely HJ, Morelli JN, Pfeuffer J, Attenberger UI, Schoenberg SO, et al. Zoomed EPI-DWI of the pancreas using two-dimensional spatially-selective radiofrequency excitation pulses. *PLoS One* 2014;9:e89468
17. Yoo RE, Lee JM, Yoon JH, Kim JH, Han JK, Choi BI. Differential diagnosis of benign and malignant distal biliary strictures: value of adding diffusion-weighted imaging to conventional magnetic resonance cholangiopancreatography. *J Magn Reson Imaging* 2014;39:1509-1517
18. Koh DM, Collins DJ, Orton MR. Intravoxel incoherent motion in body diffusion-weighted MRI: reality and challenges. *AJR Am J Roentgenol* 2011;196:1351-1361
19. Lemke A, Laun FB, Klauss M, Re TJ, Simon D, Delorme S, et al. Differentiation of pancreas carcinoma from healthy pancreatic tissue using multiple b-values: comparison of apparent diffusion coefficient and intravoxel incoherent motion derived parameters. *Invest Radiol* 2009;44:769-775
20. Alley MT, Pauly JM, Sommer FG, Pelc NJ. Angiographic imaging with 2D RF pulses. *Magn Reson Med* 1997;37:260-267
21. Kartalis N, Loizou L, Edsborg N, Segersvärd R, Albiin N. Optimising diffusion-weighted MR imaging for demonstrating pancreatic cancer: a comparison of respiratory-triggered, free-breathing and breath-hold techniques. *Eur Radiol* 2012;22:2186-2192
22. Inan N, Arslan A, Akansel G, Anik Y, Demirci A. Diffusion-weighted imaging in the differential diagnosis of cystic lesions of the pancreas. *AJR Am J Roentgenol* 2008;191:1115-1121
23. Andre JB, Zaharchuk G, Saritas E, Komakula S, Shankaranarayan A, Banerjee S, et al. Clinical evaluation of reduced field-of-view diffusion-weighted imaging of the cervical and thoracic spine and spinal cord. *AJNR Am J Neuroradiol* 2012;33:1860-1866
24. Landis JR, Koch GG. An application of hierarchical kappa-type statistics in the assessment of majority agreement among multiple observers. *Biometrics* 1977;33:363-374
25. Reischauer C, Wilm BJ, Froehlich JM, Gutzeit A, Prikler L, Gablinger R, et al. High-resolution diffusion tensor imaging of prostate cancer using a reduced FOV technique. *Eur J Radiol* 2011;80:e34-e41
26. Singer L, Wilmes LJ, Saritas EU, Shankaranarayanan A, Proctor E, Wisner DJ, et al. High-resolution diffusion-weighted magnetic resonance imaging in patients with locally advanced breast cancer. *Acad Radiol* 2012;19:526-534
27. Wheeler-Kingshott CA, Parker GJ, Symms MR, Hickman SJ, Tofts PS, Miller DH, et al. ADC mapping of the human optic nerve: increased resolution, coverage, and reliability with CSF-suppressed ZOOM-EPI. *Magn Reson Med* 2002;47:24-31
28. Wilm BJ, Svensson J, Henning A, Pruessmann KP, Boesiger P, Kollias SS. Reduced field-of-view MRI using outer volume suppression for spinal cord diffusion imaging. *Magn Reson Med* 2007;57:625-630
29. Chandarana H, Babb J, Macari M. Signal characteristic and enhancement patterns of pancreatic adenocarcinoma: evaluation with dynamic gadolinium enhanced MRI. *Clin Radiol* 2007;62:876-883
30. Kim JH, Park SH, Yu ES, Kim MH, Kim J, Byun JH, et al. Visually isoattenuating pancreatic adenocarcinoma at dynamic-enhanced CT: frequency, clinical and pathologic characteristics, and diagnosis at imaging examinations. *Radiology* 2010;257:87-96
31. Rieseberg S, Frahm J, Finsterbusch J. Two-dimensional spatially-selective RF excitation pulses in echo-planar imaging. *Magn Reson Med* 2002;47:1186-1193
32. Wang Y, Chen ZE, Yaghmai V, Nikolaidis P, McCarthy RJ, Merrick L, et al. Diffusion-weighted MR imaging in pancreatic endocrine tumors correlated with histopathologic characteristics. *J Magn Reson Imaging* 2011;33:1071-1079
33. Dowell NG, Jenkins TM, Ciccarelli O, Miller DH, Wheeler-Kingshott CA. Contiguous-slice zonally oblique multislice (CO-ZOOM) diffusion tensor imaging: examples of in vivo spinal cord and optic nerve applications. *J Magn Reson Imaging* 2009;29:454-460
34. Jeong EK, Kim SE, Guo J, Kholmovski EG, Parker DL. High-resolution DTI with 2D interleaved multislice reduced FOV single-shot diffusion-weighted EPI (2D ss-rFOV-DWEPI). *Magn Reson Med* 2005;54:1575-1579